VALIDATION OF SHOCK LAYER RADIATION: PERSPECTIVES FOR TEST CASES

Aaron Brandis

ERC Inc, at NASA Ames Research Center

ABSTRACT

This paper presents a review of the analysis and measurements of radiation data obtained in the NASA Ames Research Center's Electric Arc Shock Tube (EAST) facility. The goal of these experiments was to measure the level of radiation encountered during atmospheric entry. The data obtained from these experiments is highlighted by providing the first spectrally and spatially resolved data for high speed Earth entry and measurements of the CO 4th Positive band for conditions relevant to Mars entry. Comparisons of the EAST data with experimental results obtained from shock tunnels at JAXA and the University of Queensland are presented. Furthermore, the paper will detail initial analyses into the influence and characterization of the measured non-equilibrium radiation.

Key words: Shock layer radiation, Mars, validation, simulation, test case.

1. INTRODUCTION

The radiative component of the heat flux encountered by previous vehicles entering the Martian atmosphere has generally been negligible. However, due to future potential missions involving high mass landers and high speed entry, interest in radiative heating has recently arisen for Martian entry conditions. Detailed simulations and experiments have been undertaken to quantify this radiation and associated uncertainties [1, 2, 3, 4]. Understanding these uncertainties may influence future margin policies [5], and hence the thermal protection system (TPS) selection and thickness. The present analysis attempts to provide insight into the accuracy of theoretical models, and provide a validation of CO 4th Positive measurements performed at conditions relevant to Martian entry. The significance of CO 4th Positive radiation is highlighted in Fig. 1, where it can be seen that this band contributes approximately 65% of the total radiance at 7.96 km/s and 0.25 Torr. Furthermore, a significant portion of the CO 4th Positive band is optically thick, as can be seen in Fig. 2, where the intensity calculated without self absorption is several orders of magnitude greater than the intensity calculated with self absorption. As the absolute intensity level of CO 4th Positive is black body limited, the intensity dependence on temperature is particularly strong for two reasons. Firstly, the CO 4th Positive emission increases with increasing temperature, and secondly, as the temperature increases the black body limit increases, therefore allowing greater levels of radiative intensity to be observed. This work will attempt to characterize the data obtained from EAST and highlight the need for a thorough understanding of a shock tube's performance to allow robust facility-to-facility comparisons.

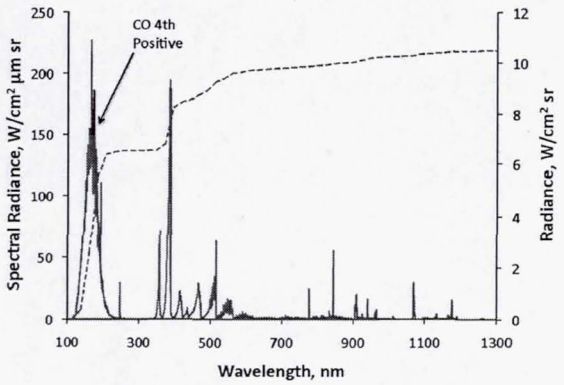

Figure 1. NEQAIR calculated spectrum for Mars entry at 7.96 km/s and 0.25 Torr highlighting contribution from CO 4th Positive.

2. DESCRIPTION OF THE EAST FACILITY

The EAST facility at NASA Ames Research Center was developed to simulate high-enthalpy, "real gas" phenomena encountered by hypersonic vehicles entering planetary atmospheres. This enables experiments to be performed with flow parameters, such as velocity, static pressure, and atmospheric composition close to actual flight conditions. The basic principle behind testing in the EAST facility is that the shock-heated test gas in a shock tube simulates conditions found behind the bow shock on a re-entry vehicle. It has the capability of producing superorbital shock speeds using an electric arc driver with a driven tube diameter of 10.16 cm [6]. The region of valid test gas lies between the shock front and the contact surface that separates the driver and driven gases. The

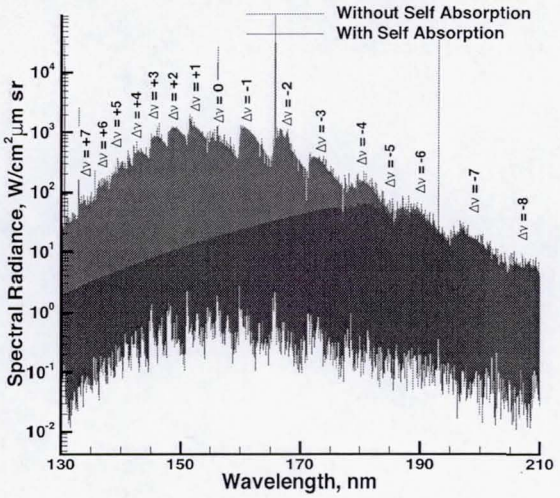

Figure 2. CO 4th Positive intensity calculated by NEQAIR using the Rodio and Hassan data with and without self absorption (path length = 10.16 cm). Band head locations are also shown.

test time is defined as the axial distance between these two points divided by the local shock velocity. The characteristics of the EAST arc driver typically result in test times of approximately 4 - 10 μs. Though short, this test time is often sufficient to capture the peak of the non-equilibrium shock radiation and the decay to equilibrium conditions. As the shocked gas arrives at the location of the test section in the tube, spectrometers attached to Charge Coupled Devices (CCDs) are gated and the spectral and spatial emission of the gas is analyzed. EAST utilizes four spectrometers per shot, associated with four different wavelength ranges. These cameras are commonly referred to as: VUV ($\sim$ 120 – 215 nm), UV/Vis ($\sim$ 190 nm – 500 nm), Vis/NIR ($\sim$ 480 nm – 900 nm) and IR ($\sim$ 700 nm – 1650 nm).

3. DESCRIPTION OF PREDICTIVE CODES AND DATABASES

Simulations were conducted with three separate radiation codes, NEQAIR [7], HARA[8, 9] and HyperRad [10]. Figure 3 shows a comparison of the NEQAIR and HARA codes using the CO 4th Positive data calculated by Babou et al [11]. HyperRad is not shown here because it uses its own database. It can be seen that both codes produce very similar spectra and integrated radiance (a difference of less than 1%) when using the same database [12]. The differences between the two calculated spectra are due to the different line-shapes implemented in the spectral convolutions of NEQAIR and HARA. As the differences between the two codes are small, this paper will not focus on comparing calculations performed with different codes, but rather on the different databases used

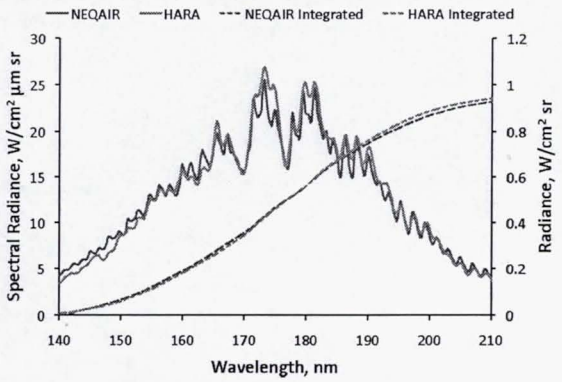

Figure 3. Comparison of CO 4th Positive calculated by NEQAIR and HARA using the Babou et al. data at 6.45 km/s and 0.25 Torr.

for CO 4th Positive that could be implemented in either code. Three different databases are used with NEQAIR and HARA, as discussed below, while HyperRad employs its own newly developed *ab initio* database.

3.1. NEQAIR Code

NEQAIR is a line-by-line radiation code the name of which stands for Non-equilibrium Air Radiation. NEQAIR computes spontaneous emission, absorption and stimulated emission due to transitions between various energy states of chemical species along a line-of-sight. Individual electronic transitions are considered for atoms and molecules, with the molecular band systems being resolved for each rotational line. The process for conducting the NEQAIR simulations is to perform the calculation at a very high spectral resolution followed by a convolution (scan) with a slit function. The slit function is a combination of a Lorentzian and Gaussian function that has been fit to the corresponding measured instrument line shape. More detail about NEQAIR and the instrument line shape can be found in Whiting et al. [7] and Cruden et al. [13], respectively.

3.2. HARA Code

The HARA radiation model applied in the present study is discussed in detail by Johnston et al.[8, 9] This model is based on a set of atomic levels and lines obtained from the National Institute of Standards and Technology (NIST)[14] and Opacity Project databases.[15] The atomic bound-free model is composed of cross sections from the Opacity project's online TOPbase,[16] which were curve fit by Johnston.[8] As CO 4th Positive is optically thick, a line-by-line approach for molecular radiation has been implemented into HARA.

3.3. HyperRad Code

HyperRad is a radiation code being developed at NASA Ames Research Center to compute fully coupled radiative heating of the gas and body surfaces in hypersonic flow and to provide spectra for comparison to experiment and flight data. The reason for the development of HyperRad is to extend and update the physics utilized in codes such as NEQAIR and HARA and to include data from recent *ab initio* calculations. The physics-based modelling for energy state populations implemented in HyperRad uses coupled thermal, chemical, and radiative nonequilibria and is designed for high-end computing in terms of efficiency and parallelization. An efficient and accurate, linelist-driven database has been implemented that contains data merged from NIST [14], Vanderbilt [17] and TOPBase [16] atomic line datasets. The database currently includes C, C^+, N, N^+, O, O^+; and the molecular band systems N_2, O_2, N_2^+, NO, C_2, CO, CO^+, CN, C_3, CO_2, C_2H. *Ab initio* calculations are used for electric dipole and quadrupole, magnetic dipole, and spin-forbidden transitions which include fine structure, predissociation, and non-adiabatic corrections. The line broadening and shifts due to the Stark effect are based on computed rate coefficients and the line-widths have been parameterized up to a temperature of 50,000 K. More details regarding the development of the HyperRad code and database will be presented in upcoming publications.

3.4. Overview of CO 4th Positive Models

Various CO 4th Positive databases have been implemented into both NEQAIR and HARA for the purposes of comparison with EAST. The CO 4th Positive databases used in this paper have been compiled by Rodio and Hassan [18, 19, 20], Babou et al. [11] and da Silva and Dudeck [21]. The methodologies for calculating the spectroscopic data are similar in all three cases. Each method involves calculating Franck-Condon factors (FCF) and Hönl-London factors within the Born-Oppenheimer approximation [22]. However, there are differences between the methods. For example, Rodio and Hassan use the R-centroid approximation while Babou et al. and da Silva and Dudeck take into account the dependency of the Electronic Transition Moment Function (ETMF) on the inter nuclei distance. Furthermore, there are differences in the various sources of literature used for the calculation of the spectroscopic data. Two such differences relate to the method used for calculating the potential energy curves and the choice in the source of data used for the ETMF. In terms of calculation of the potential energy curves, Rodio and Hassan implement a 5 parameter Hulburt-Hirschfelder potential [23], whereas both Babou et al. and da Silva and Dudeck use the Rydberg-Klein-Rees (RKR) [24, 25, 26] procedure. In terms of the choice of ETMF implemented, Babou et al. use the *ab initio* ETMF developed by Kirby and Cooper [27], while da Silva and Dudeck, and Rodio and Hassan use the experimentally based ETMF developed by DeLeon [28].

In terms of the calculation of CO 4th Positive emission with HyperRad, the theoretical spectrum is based on high quality *ab initio* potential energy curves and transition moments computed using the Molpro program [29]. The *ab initio* calculations utilized the cc-pV5Z [30] one electron basis set augmented by the correlating functions and diffuse basis functions as advocated by Schwenke [31]. The molecular orbitals were generated by the complete active space method using the valence active space and weighted averages of various energy states. These weights were dynamically determined as described by Deskevich et al [32]. The final energies and transition moments were computed using the averaged coupled pair functional method correlating all electrons. The ro-vibrational energy levels and transition energies were computed using the code previously described by Schwenke [33]. To improve the agreement with experimental measurements, the $B^1\Pi$ potential was shifted downwards by 120 cm^{-1} to make the computed and measured $\nu = 2$ and $J = 1$ energy the same. The measured energy is 67678.92 cm^{-1}, so the adjustment is less than 0.2%.

4. EAST DATA

A breakdown of the Mars conditions tested in the EAST facility are provided in Table 1. The table shows that there has been an effort to cover a wide range of conditions, and so the data set provides a strong basis for determining future test cases. The presently defined test case, TC2-M5, focuses on conditions at 0.1 and 1.0 Torr with a range of shock speeds from 7 to 8 km/s. Ideally a test case will allow comparisons to be conducted under both equilibrium and nonequilibrium conditions. Unfortunately, in the case of the 0.1 Torr Mars testing in EAST, the contamination often arrives before the flow reaches a complete equilibrium state. In the case of the 1.0 Torr condition, the pressure is sufficiently high, that nonequilibrium begins to play a less significant role. Furthermore, at 1.0 Torr, CN Violet is not optically thin and so makes comparisons of facilities with different diameters more complex. Therefore, a good choice for a future test case could be based at a pressure of 0.25 Torr with shock speeds ranging from approximately 6.5 to 8 km/s.

The main spectral features of interest for this paper are the CO 4th Positive emission between 120 and 240 nm and the CN Violet emission between 340 and 430 nm. It should be noted that the VUV is a very difficult region to obtain spectral data due to the absorption of the emitted radiation by ambient oxygen below 190 nm. Therefore, the collection optics and spectrometer need to be located in a vacuum environment, and special windows are required to allow the transmission of data (UV-Silica for > 165 nm, sapphire for > 145 nm, and LiF or MgF_2 for > 120 nm). As the VUV spectrometer is unable to cover the entire CO 4th Positive band in one shot at a suitable spectral resolution, the experiments have focused on the emission between 145 and 195 nm. Furthermore, a number of experiments were performed to capture the

Table 1. Breakdown of EAST Mars Shots

Pressure (Torr)	# Shots	Min Shock Speed (km/s)	Max Shock Speed (km/s)
0.01	2	9.0	9.7
0.05	4	7.2	7.8
0.10	31	6.0	8.8
0.20	8	3.9	10.0
0.25	24	6.3	8.1
1.00	34	3.0	8.3
Total	**103**		

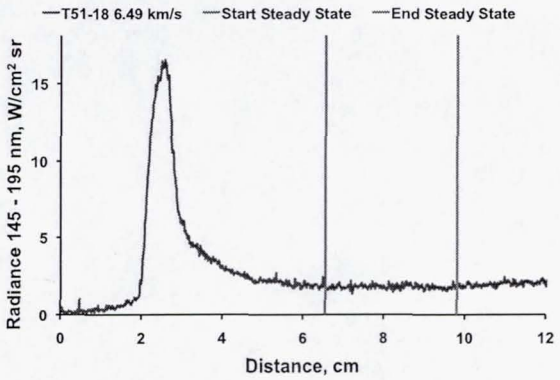

Figure 4. Radiance integrated over CO 4th Positive from 145 - 195 nm versus distance at 0.25 Torr and 6.29 km/s

black body limited deep VUV spectra of CO 4th Positive while simultaneously capturing the "red side" tail of CO 4th Positive on the UV/Vis spectrometer. Figure 4 shows the radiance integrated over the CO 4th Positive band emitting between 145 and 195 nm [12]. The data shows a shot reaching a steady state of radiance between 6 to 10 cm. This shot would be assigned an equilibrium rating of 4 (out of 5) according to the classification specified by Brandis et al [34]. The reason for this shot not being given an equilibrium rating of 5 is due to the relatively significant level of noise found in the steady state regions.

5. COMPARISON OF PREDICTIONS AND EAST

Figure 5 shows a comparison of EAST CO 4th Positive radiative intensity data with results generated by HyperRad and with the databases compiled by Rodio and Hassan, Babou et al. and da Silva and Dudeck. All four cases have been calculated using the CEA calculated equilibrium temperature. The CO 4th Positive is shown centered on the spectrometer showing emission from 145 - 195 nm. A 3-point moving average has been applied to the EAST results obtained from the VUV camera to remove some of the pixel-to-pixel noise. The emission between 120 and 165 nm is almost completely limited by the black body curve. Therefore, the radiance in this spectral range should be purely a function of temperature. From 165 - 195 nm, portions of the spectrum are black body-limited. Under the finite spectral resolution of the experimental measurements, these regions are smeared out to lie below the black body curve, but are still strongly impacted by the temperature due to self-absorption of the line peaks.

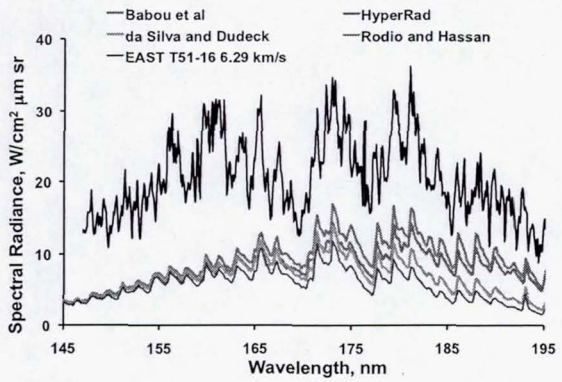

Figure 5. Comparison of various databases and EAST for CO 4th Positive emission at 0.25 Torr using the CEA calculated equilibrium temperature.

The first observation that can be clearly seen from Fig. 5 is that the black body limited region of the spectrum is significantly under-predicted. This implies that the CEA equilibrium temperature is less than the actual flow temperature [12]. In particular, the impact can be seen across the spectral region between 145 and 160 nm for all the databases implemented. However, for some shots, the CEA equilibrium properties do produce a good comparison with EAST between 170 – 195 nm and 190 – 230 nm with both the Babou et al. database and HyperRad. However, the mismatch in the black body region observed for these shots suggests this agreement may be fortuitous [12].

As the EAST data is limited by the black body curve between 145 - 155 nm, the temperature of each experiment can be extracted from the data by matching the slope and intensity of this portion of the spectrum. In order to match the black body limited portion of the spectrum, a methodology was developed to perform simulations using a temperature greater than the equilibrium value calculated by CEA. This methodology is as follows [12]:

1. CEA is used to calculate the post shock conditions based on the experimentally measured shock speed, initial temperature and pressure of the test gas.
2. An initial guess of the black body temperature is obtained by fitting a black body curve to the upper limit

of EAST data for wavelengths up to 155 nm.

3. This initial temperature is then used as a first guess for an iterative process using NEQAIR to obtain the best fit through the EAST data for wavelengths up to 155 nm.

4. With the new experimental black body temperature, the post shock density of the flow is decreased by the same relative amount that the temperature of the flow was increased, thereby maintaining the same pressure.

5. A new temperature-volume CEA calculation is performed using the updated flow density and temperature to calculate the new state of the post shock conditions.

Calculations performed with the black body temperature extracted from an EAST experiment are shown in Fig. 6 [12]. The amount of temperature increase required was 460 K greater than the equilibrium temperature calculated by CEA. The temperature increase is not consistent from shot to shot, as shown in Fig. 7. Figure 7 shows the percent increase from equilibrium temperature to black body temperature for 14 shots from EAST and 1 shot from HVST at different shock speeds and initial pressures. The figure shows that there is no trend between the percent increase in temperature and shock velocity or pressure. The temperature increase required could be less significant on HVST than on EAST, but more shots from HVST would be required to confirm this.

Figure 6 shows that when using the Rodio and Hassan, and da Silva and Dudeck databases, combined with increasing the temperature to match the black body limit, the overall agreement between the simulation and experiment is generally very good [12]. However, there are a few discrepancies evident across all the conditions. These differences include an over-prediction of EAST between approximately 165 - 170 nm with both Rodio and Hassan, and da Silva and Dudeck databases and an under-prediction of EAST between approximately 180 - 195 nm with the Rodio and Hassan database. When using the Babou et al. database and HyperRad, even though the agreement is still maintained from 145 - 160 nm (the black body limited region), there is a substantial over-prediction of EAST from 160 - 195 nm. A possible explanation for the over-prediction of these two databases would be justified if there were to be a non-boltzmann population of the high vibrational energy transitions of CO, thus affecting the transitions corresponding to the bands emitting from 160 nm and longer [12]. It is only the high vibrational energy transitions that can be validated with these EAST results as the transitions from a $\Delta\nu = -3$ and higher are completely black body limited (as was indicated in Fig. 2).

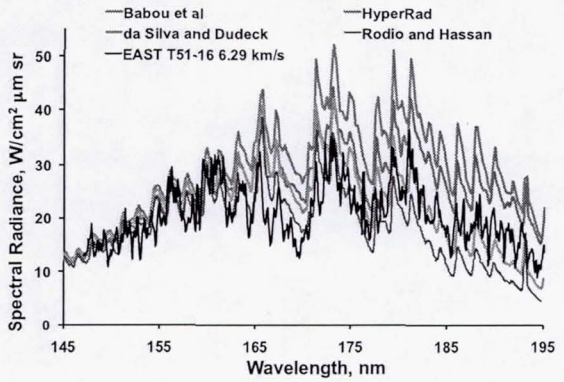

Figure 6. Comparison of various databases and EAST for CO 4th Positive emission at 0.25 Torr using a temperature increase of 460 K compared to CEA equilibrium.

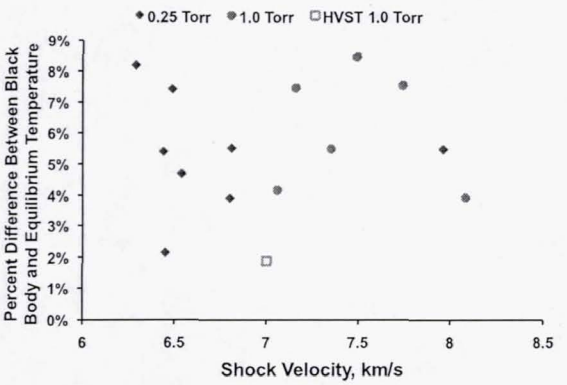

Figure 7. Percent increase required to match experimental black body compared to CEA equilibrium.

5.1. Validation of Temperature Increase

In order to increase confidence in performing simulations using the black body temperature extracted from the EAST data, the influence of this temperature increase on the Vis/NIR and IR spectral data acquired from the same shots coinciding with the CO 4th Positive data has been analyzed [12]. The IR region is dominated by atomic C lines with a broad emission from CN Red. The results for the IR spectral region are shown in Fig. 8(a) and coincide with a shot where a temperature increase of 374 K compared to equilibrium was required to match the black body limited spectral region. It can be seen from the figure that there is substantial improvement in terms of the agreement with EAST when the temperature increase is implemented. When the temperature of the flow is increased, the simulation agrees to within 10%, whereas the equilibrium solution is a factor of 2.1 lower [12]. It should also be noted that a small increase in temperature can drastically change the number density of a species, as shown in Fig. 8(b). Figure 8(b) shows the variation of number densities for species that are significant to the total radiation for the conditions presented in this paper at a constant density of 0.01 kg/m^3. For example, an increase in temperature from 5500 K to 6000 K corresponds to an increase in C_2 number density by a factor of 14.

The effect of the temperature increase on the simulations for the Vis/NIR spectral region (dominated by emission from C_2 Swan and CN Red) is shown in Fig. 9. In all cases the integrated Vis/NIR radiance is closer to the experimental result when the temperature is increased [12]. Figure 9 shows that when the temperature is increased, although the agreement is improved for the 575 - 875 nm (CN Red) region compared to equilibrium, there is still substantial room for improvement. The disagreement in this spectral region has also been observed by Cruden et al [1]. However, in contrast, it can be seen in the figure that the C_2 Swan bands between 475 - 575 nm and the atomic Oxygen line at 777 nm show greatly improved agreement with EAST when using the increased temperature in the simulations.

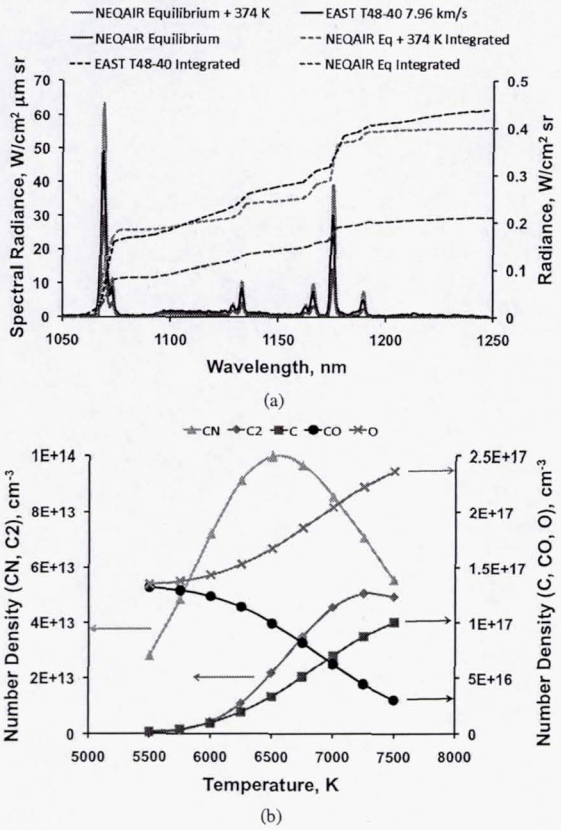

Figure 8. (a) Comparison of NEQAIR and EAST for the Infra-Red spectral region at 0.25 Torr. (b) Species number density as a function of temperature at 0.01 kg/m^3.

5.2. Summary of Results

Figure 10 summarizes the comparisons of CO 4th Positive radiance obtained at 0.25 Torr integrated over 145 to 195 nm using the CEA equilibrium temperature and using the black body temperature extracted from EAST [12]. Figure 10(a) shows that for 4 of the EAST shots, all databases significantly under-predict the integrated experimental result when the equilibrium temperature is used. However, when the temperature is increased to match the black body limited portion of the EAST spectra, as shown in Fig. 10(b), the databases bound the experimental result. It can also be seen from these figures that the two databases that use an experimental based ETMF (Rodio and Hassan, and da Silva and Dudeck) produce a smaller integrated value of radiance when compared to HyperRad and Babou et al., both of which use

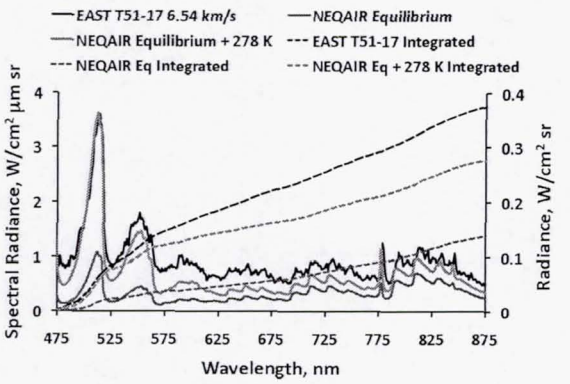

Figure 9. Comparison of NEQAIR and EAST for the Vis/NIR spectral region at 0.25 Torr and 6.54 km/s

an ETMF based on *ab initio* calculations. Figure 10(b) also shows the results of an analysis related to the uncertainty in temperature due to the calculation of shock speed for each shot. Each data point shown in the figure shows the percentage temperature increase used in the calculations and next to this number in parentheses is the corresponding uncertainty in temperature due to the uncertainty in the measurement of the shock speed, using an estimated shock speed uncertainty of 1%. The uncertainty in temperature due to shock speed is around 1 – 1.5%, while the uncertainty in temperature due to the absolute radiance calibrations is approximately 1.5%. The temperature mismatch however, varies from 2 - 9%, so may only partly be explained by these experimental uncertainties [12]. Furthermore, these experimental errors are expected to be normally distributed while the temperature trend shows a bias towards a higher temperature. This, in combination with the discussion of Sect 5.1, suggests the temperature increase is a real phenomenon in the shock tube. Potential theories for this increase relate to either the driver gas heating the test gas, viscous flow effects causing the deceleration of the shock or expansion waves originating at the driver impinging on the test gas. However, reasons for this are not yet fully understood.

6. FACILITY TO FACILITY COMPARISON

The goal of the TC2-M5 test case was to provide data at defined Mars entry conditions (0.1 and 1 Torr, at velocities of 7, 7.5 and 8 km/s) from three shock tubes: X2 at The University of Queensland, HVST at JAXA and EAST at NASA Ames Research Center. These three facilities have been chosen as they can all provide data at conditions relevant to Mars entry. The dimensions of the three facilities are similar, with X2 having a diameter of 8.5 cm, HVST a width of 7 cm (square tube) and EAST having a diameter of 10.16 cm. Data from EAST specifically pertaining to these defined test cases was presented by Cruden [35]. At the time of publishing, specific test case data was not available from either X2 or HVST. However, data has previously been reported for Mars conditions in X2 by Brandis [4], and in HVST by Takayanagi [3]. A plot of the integrated equilibrium CN Violet data obtained at from all three facilities is shown in Fig. 11. The uncertainties shown in this figure have been defined as follows: for EAST the uncertainty in radiance is 17% and for shock speed is 1% [34], for X2 the uncertainty in radiance is 25% and for shock speed is 2.5%[4], while the the uncertainty for HVST has been set to be the same as for X2 as it was not defined in the reference containing the data. NEQAIR results are also shown to provide a reference point as the experiments are not at the same shock speed. This comparison highlights the benefit of running a variety of shock speeds for a test case, as it is unlikely the exact shock speed will be replicated in all three facilities. However, if the experiments are focused to cover a range of shock speeds, the trends in the data can be compared. It can be seen from the figure that at 1.0 Torr the EAST data has significantly less variability than at 0.1 Torr, and all data points are generally within

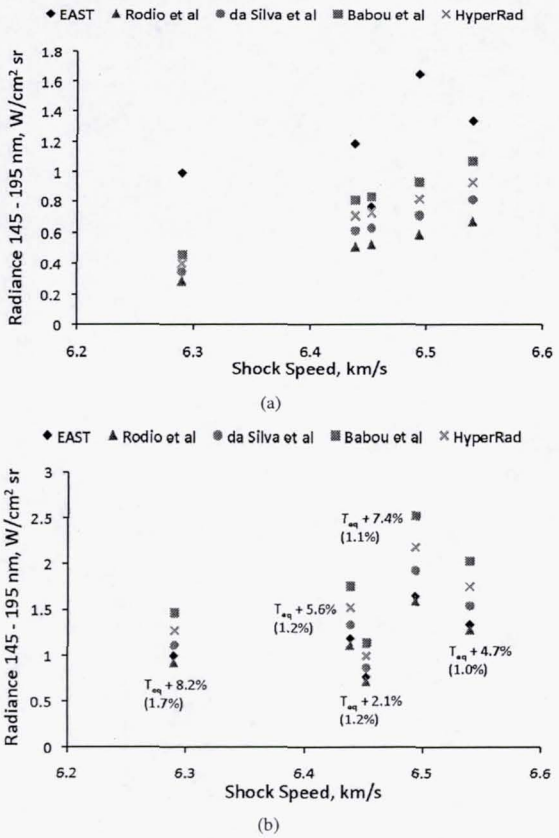

Figure 10. Summary of the comparison of the various databases and EAST for CO 4th Positive emission at 0.25 Torr at (a) equilibrium temperature (b) experimental black body temperature (also showing percent increase in equilibrium temperature, and corresponding uncertainty in temperature due to the uncertainty in shock speed).

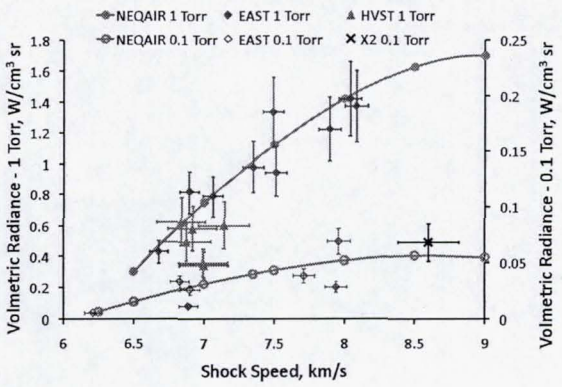

Figure 11. Comparison of results from EAST, HVST, X2 and NEQAIR for CN Violet in Mars conditions.

the designated uncertainty. The reason for the increased variability in the 0.1 Torr data is due to the fact that, in the EAST facility, the arrival of the contamination front often limits the test gas from reaching a true equilibrium state. This is particularly true for the UV/Vis spectral region due to the long relaxation times of CN Violet. It can also be seen that the data obtained from HVST and X2 is generally in good agreement with NEQAIR (3 of the 6 data points for HVST and the 1 data point from X2 are within their designated uncertainty compared to NEQAIR). Therefore, as both HVST and X2 agree well with NEQAIR, it can then be deduced that both facilities show good agreement to the results obtained from EAST. It should also be noted that this analysis is based on the assumption that the CN Violet emission is optically thin. The significance of self absorption was tested by performing a NEQAIR calculation at 7 km/s and 1 Torr. The results showed that there was a 4 % increase in the NEQAIR result when a path length of 7 cm was used (as in HVST) compared to a path length of 10.16 cm (as in EAST). This difference was deemed to be negligible for the purposes of this paper.

7. NONEQUILIBRIUM METRICS

Many insights into the level of agreement between simulations and experimental results have been made possible by analyzing integrated equilibrium spectra across a range of conditions and comparing the trends [12]. However, for nonequilibrium, it is not immediately clear that one parameter can describe the level of nonequilibrium intensity observed in each shot over a large range of conditions. This is because the temporal intensity trace changes significantly as the underlying physics changes with different shock speeds. This section will analyze the benefits and drawbacks of three proposed methods for determining a parameter that highlights the significance of the nonequilibrium radiative intensity. In the best case scenario, the nonequilibrium parameter would be: 1) Independent of experimental parameters (such as gate width and spatial resolution, 2) Applicable to a wide range of conditions, 3) Easily comparable to simulation results, 4) Consistent with limitations of test time in the facility and 5) Able to be normalized by the equilibrium value. The proposed metrics to summarize the level of nonequilibrium in a single parameter are indicated in Fig. 12. The options plotted all indicate a metric that revolves around integrating a portion of the intensity trace. Integrating the trace is suggested as a more robust way to conduct a comparison as opposed to using a peak intensity, as the comparisons are then not bound to experimental parameters such as gate opening times and spatial smearing due to shock movement. The three options shown in Fig. 12 are: 1) Integrate the intensity from 2 cm before the shock peak until equilibrium is reached, Fig. 12(a), 2) Integrate the area of intensity above the nominal equilibrium level, Fig. 12(b) and 3) Integrate the intensity some fixed distance either side of the shock, Fig. 12(c). Here, $\pm$ 2 cm is chosen based on observed worst case test time limitations and the rise time of the shock. [36]

To conduct the most robust nonequilibrium comparisons possible, it would be advantageous for the nonequilibrium metric to be able to be normalized to the equilibrium level, as is the case with the 1st and 2nd metrics. By normalizing the metric to the equilibrium level, any uncertainty due to the absolute intensity calibration is divided out of the analysis. A value that is the integrated nonequilibrium area normalized by the equilibrium level would give an indication to the significance of the nonequilibrium to the total radiative flux. However, unlike, metric 3, metrics 1 and 2 can not be assigned to all shots. Both metric 1 and 2 require a steady state region of the flow to be identified. Furthermore, metric 2 is best applied to a shot showing a relatively strong nonequilibrium region behind the shock, as it can not be applied to a shot when equilibrium is very quickly reached behind the shock (such is found at high shock speeds, $\approx>$ 12 km/s). The advantage of the 3rd metric is that it can be applied to almost all shots (provided that the shot has at least 2 cm of test time), even if the flow doesn't reach a steady state. Therefore, this metric is particularly applicable to low pressure shots where the data from EAST often does not reach a complete equilibrium or steady state value (see the 0.1 Torr trace in Fig. 12(c)). Another advantage of the 3rd metric is that if the flow is optically thin, it would derive a "flight-relevant" heating value for a vehicle with approximately a 2 cm shock standoff distance. However, one problem with this metric can be if the flow has reached equilibrium within 2 cm following the peak intensity location (as is the case for the 1 Torr trace in Fig. 12(c)), as the integrated area would be dominated by equilibrium radiation.

Examples of metrics 1 and 3 being applied to CN Violet as measured on the EAST and X2 facilities and are presented in Fig. 13. Figure 13(a) shows the 1st metric with the integrated data being scaled by the equilibrium level. The physical interpretation of this nonequilibrium distance is that it corresponds to the length of equilibrium/steady-state radiance to be equivalent to the

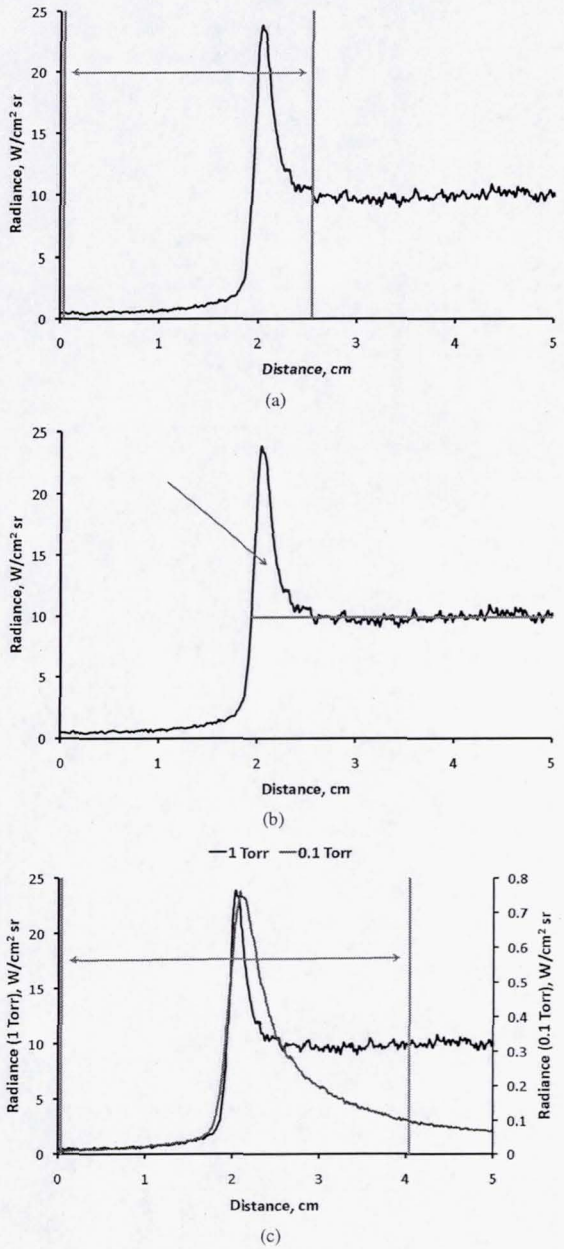

Figure 12. Examples of different metrics to characterized the level of nonequilibrium. (a) Integrating the intensity from 2 cm before the shock peak until equilibrium is reached, (b) Integrating the area of intensity above the nominal equilibrium level, and (c) Integrating the intensity from 2 cm before the shock peak until 2 cm after the shock peak.

amount of nonequilibrium radiation. The results shown in this figure correspond to what is intuitively expected, as the significance of the nonequilibrium radiation is seen to reduce substantially as pressure and velocity are increased. The 3rd metric is shown in Fig. 13(b), where it can be seen that the data is self consistent and behaves as expected with respect to velocity and pressure. The figure shows the absolute value of nonequilibrium radiation increasing with both increasing pressure and velocity. More data points can be seen in Fig. 13(b) compared to Fig. 13(a), particularly at 0.1 Torr. This is due to the 1st metric requiring a steady state value of radiance to be defined, which is often not observed at 0.1 Torr in EAST. Results shown in these figures indicate that the level of nonequilibrium measured on X2 is similar to that measured on EAST. This is particularly the case when the 1st metric is used. As the 1st metric is independent of the absolute intensity calibration, the fact that better agreement is seen with metric 1 rather than metric 3, indicates that there could be a small calibration error with one of the facilities. It can also be concluded from these initial analyses of the nonequilibrium trends that none of the proposed metrics is applicable across all conditions that were analyzed. The effectiveness of each of the metrics compared to the five criteria highlighted earlier in this section is summarized in Table 2.

Table 2. Summary of effectiveness of nonequilibrium metrics.

	Independent of Exp. Parameters	Wide Range of Conditions	Easily Comparable	Test Time Limits	Normalized to Equilibrium
Metric 1 -2cm to start of equilibrium	Yes	OK	No	OK	Yes
Metric 2 area above equilibrium	Yes	No	Yes	OK	Yes
Metric 3 -2cm to +2 cm	Yes	Yes	Yes	Yes	No

8. CONCLUSION

Measurements of CO 4th Positive radiative intensity have been made across a range of conditions in the EAST facility with the results being compared against four CO 4th Positive databases compiled and calculated by Rodio and Hassan, Babou et al., da Silva and Dudeck and Hy-

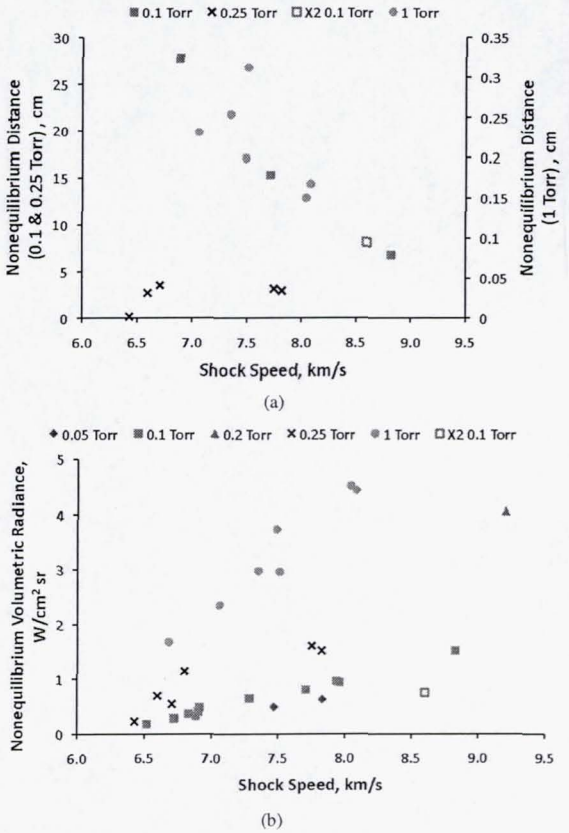

Figure 13. Examples of nonequilibrium results for CN Violet using (a) metric 1 and (b) metric 3.

perRad. Initial comparisons were conducted using equilibrium conditions as calculated by CEA. However, it has been shown in this paper that the predicted equilibrium temperature significantly under-predicts the EAST data, in particular, the spectral region of EAST where the intensity is limited by the black body curve. This spectral region should be purely a function of temperature and has been shown to be under-predicted for all the 0.25 Torr conditions presented in this paper. As the intensity measured on EAST in the spectral region from 130 - 155 nm is limited by the black body curve, it enables a relatively accurate measurement of the experimental flow temperature. This temperature was found to be 2 - 9% higher than the CEA equilibrium calculated value. Therefore calculations were performed with both the black body temperature extracted from each EAST shot and at the equilibrium value. Overall, the simulations performed at CEA equilibrium under-predict the experiment by an average of approximately 40%. When the simulations use the increased temperature extracted from the black body limited radiation from EAST, the results agree on average within approximately 15%. The need for the temperature increase has been further validated by comparing the influence of the increase in temperature in other spectral regions. Initial comparisons have also been made for CN Violet between 3 shock tube facilities, EAST at NASA Ames Research Center, HVST at JAXA and X2 at the University of Queensland. Using NEQAIR as a baseline, all 3 facilities showed good agreement with each other, as almost all data points are within their experimental uncertainty compared to the simulation results. Three proposed metrics to define a single parameter summarizing the significance of the nonequilibrium radiation was analyzed. It was shown in this paper that the metrics will be useful for future comparisons with simulations and experiments. However, no one individual metric was found to be able to cover all possible conditions. Therefore, each metric must be used according to the characteristics of each intensity trace. Finally, it has been proposed in this paper that a good future test case would be to focus on conditions at 0.25 Torr and shock speeds ranging from 6.5 to 8 km/s. At 0.25 Torr, the EAST shots display both a good level of equilibrium while still having a significant portion of the flow in nonequilibrium. It has been highlighted in this paper that there are issues with both 0.1 and 1.0 Torr being used as test case conditions. At 0.1 Torr, the EAST shots seldom reach equilibrium/steady state, while at 1.0 Torr the level of nonequilibrium is relatively insignificant. Furthermore, at 1.0 Torr, CN Violet is no longer optically thin, and therefore makes comparisons between facilities with different diameters more challenging.

ACKNOWLEDGMENTS

The author would like to acknowledge to the work and useful discussion with Drs Brett Cruden, Dinesh Prabhu, Chris Johnston, Alan Wray, Yen Liu and David Schwenke. The Fundamental Aeronautics Hypersonics program, AAP discipline is acknowledge for finan-

cial support of the work, and Prof Thierry Magin is acknowledge for the financial support of the travel to the workshop. The author is supported by NASA contract NNA10DE12C to ERC Corporation.

REFERENCES

[1] B. Cruden, D. Prabhu, R. Martinez, H. Le, J. Grinstead, and D. Bose. Absolute radiation measurement in high mass Venus and Mars entry conditions. In *10th AIAA/ASME Joint Thermophysics and Heat Transfer Conference*, volume AIAA-2010-4508, pages 1–15, Chicago, Illinois, 2010.

[2] J. Grinstead, M. Wright, M. Wilder, D. Bogdanoff, and G. Allen. Shock radiation measurements for Mars aerocapture radiative heating analysis. *Journal of Thermophysics and Heat Transfer*, 23(2):249–255, 2009.

[3] H. Takayanagi and K. Fujita. Shock radiation measurements from Carbon Dioxide flow from VUV to IR region. In *42nd AIAA Thermophysics Conference*, volume 2011-3631, Honolulu, Hawaii, 2011.

[4] A. Brandis. *Experimental Study and Modelling of Non-equilibrium Radiation During Titan and Martian Entry*. PhD thesis, University of Queensland, Brisbane, Australia, 2009.

[5] I. Cozmuta, M. Wright, B. Laub, and W. Wilcoxson. Defining ablative thermal protection system margins for planetary entry vehicles. In *42nd AIAA Thermophysics Conference*, volume AIAA-2011-3757, pages 1–27, Honolulu, HI, 2011.

[6] J. Grinstead, J. Olejniczak, M. Wilder, D. Bogdanoff, G. Allen, and R. Lilliar. Shock-heated air radiation measurements at lunar return conditions. In *46th AIAA Aerospace Sciences Meeting and Exhibit*, volume AIAA 2008-1244, pages 1–10, 7-10 January 2008, Reno, Nevada 2008.

[7] E.E. Whiting, L. Yen, J.O. Arnold, and J.A. Paterson. NEQAIR96, nonequilibrium and equilibrium radiative transport and spectra program: Users manual. Technical Report NASA RP-1389, Ames Research Center, Moffet Field, Moffet Field, 1996.

[8] C. Johnston, B. Hollis, and K. Sutton. Spectrum modeling for air shock-layer radiation at lunar-return conditions. *Journal of Spacecraft and Rockets*, 45(5):865–878, Sep-Oct 2008.

[9] C. Johnston, B. Hollis, and K. Sutton. Non-boltzmann modeling for air shock layers at lunar return conditions. *Journal of Spacecraft and Rockets*, 45(5):879–890, Sep-Oct 2008.

[10] D. Schwenke, A. Wray, and Y. Liu. Private communication, 2011.

[11] Y. Babou, P. Riviere, M.-Y. Perrin, and A. Soufiani. Spectroscopic data for the prediction of radiative transfer in CO_2-N_2 plasmas. *Journal of Quantitative Spectroscopy and Radiative Transfer*, 110(1-2):89 – 108, 2009.

[12] A. Brandis, C. Johnston, B. Cruden, D. Prabhu, A. Wray, Y. Liu, D. Schwenke, and D. Bose. Validation of CO 4th positive radiation for Mars entry. In *AIAA*, volume AIAA 2012-1145, Nashville, Tennessee, January 2012.

[13] B. Cruden, R. Martinez, and H. Le. Electron density measurement in reentry shocks for lunar return. *Journal of Thermophysics and Heat Transfer*, 26(2):222–230, 2012.

[14] Yu Ralchenko. NIST atomic spectra database, version 3.1.0, http://physics.nist.gov/physrefdata/asd/, July 2006. last accessed September 3rd, 2007.

[15] The Opacity Project Team. *The Opacity Project*, volume 1. Bristol and Philadelphia: Institute of Physics Publishing, 1995.

[16] W. Cunto, C. Mendoza, F. Ochsenbein, and C.J. Zeippen. Topbase at the cds, http://vizier.u-strasbg.fr/topbase/topbase.html. *Astronomy and Astrophysics*, 275:L5–L8, August 1993.

[17] C. Froese Fischer and G. Tachiev. Mchf/mcdhf collection, version 2. [online]. available: http://physics.nist.gov/mchf, National Institute of Standards and Technology, Gaithersburg, MD, 2011.

[18] J. Rodio and H. Hassan. Spectroscopic data and model prediction for Venus and Mars atmospheres. In *42nd AIAA Thermophysics Conference*, volume AIAA-2011-3949, pages 1–23, Honolulu, HI, 2011.

[19] D. Prabhu. Vibrational energies of diatomic molecules using the finite-element method. Technical report, National Aerospace Laboratories, April 1995.

[20] Y. Liu, F. Shakib, and M. Vinokur. A comparison of internal energy calculation methods for diatomic molecules. *Physics of Fluids A*, 2(10):1884–1902, 1990.

[21] M. Lino da Silva and M. Dudeck. Arrays of radiative transition probabilities for plasmas. *Journal of Quantitative Spectroscopy and Radiative Transfer*, 102(3):348 – 386, 2006.

[22] I. Kovacs. *Rotational structure in the spectra of diatomic molecues*. American Elsevier Publishing Company, 1969.

[23] H. Hulburt and J. Hirschfelder. Potential energy functions for diatomic molecules. *The Journal of Chemical Physics*, 9:61–69, 1940.

[24] R. Rydberg. Graphische darstellung einiger bandenspektroskopischer ergenbnisse. *Zeitschrift für Physik A Hadrons and Nuclei*, 73:376–385, 1931.

[25] O. Klein. Zur berechnung von potentialkurven fur zweiatomige molekule mit hilfe von spektraltermen. *Zeitschrift für Physik A Hadrons and Nuclei*, 76:226–235, 1932.

[26] A. Rees. The calculation of potential-energy curves from band-spectroscopic data. *Proceedings of the physical society*, 59:998–1008, 1947.

[27] K. Kirby and D. Cooper. Theoretical study of low lying $^1\Sigma^+$ and $^1\Pi$ states of CO. II. Transition dipole moments, oscillator strengths, and radiative lifetimes. *Journal of Chemical Physics*, 90:4895–4902, 1988.

[28] R. DeLeon. CO(A-X) electric dipole transition moment. *Journal of Chemical Physics*, 89:20–24, 1988.

[29] H. Werner, P. Knowles, G. Knizia, F. Manby, M. Schutz, et al. Molpro, version 2010.1, a package of *ab initio* programs, see http://www.molpro.net, 2011.

[30] T. Dunning. Gaussian basis sets for use in correlated molecular calculations. I. the atoms boron through neon and hydrogen. *The Journal of Chemical Physics*, 90:1007–1023, 1989.

[31] D. Schwenke. A new paradigm for determining one electron basis sets: core-valence basis sets for C, N and O. *Molecular Physics*, 108, 2010.

[32] M. Deskevich, D. Nesbitt, and H. Werner. Dynamically weighted multiconfiguration self-consistent field: Multistate calculations for F + H_2O $\leftrightarrow$ HF + OH reaction paths. *The Journal of Chemical Physics*, 120:7281–7289, 2004.

[33] D. Schwenke. Opacity of TiO from a coupled electronic state calculation parametrized by *ab initio* and experimental data. *Faraday Discussions*, 109:321–334, 1998.

[34] A. Brandis, C. Johnston, B. Cruden, D. Prabhu, and D. Bose. Uncertainty analysis of NEQAIR and HARA predictions of air radiation measurements obtained in the EAST facility. In *42nd AIAA Thermophysics Conference*, volume 2011-3478, pages 1–14, Honolulu, Hawaii, 2011.

[35] B. Cruden. Recent progress in entry radiation measurements in the NASA Ames Electric Arc Shock Tube facility. In *5th International Workshop on Radiation of High Temperature Gases in Atmospheric Entry*, Barcelona, Spain, October 2012.

[36] B. Cruden. Radiance measurement for low density mars entry. In *AIAA*, volume AIAA 2012-2742, New Orleans, Louisiana, June 2012.